

CONFERENCES AND SYMPOSIA

PACS numbers: **07.60.–j**, 07.85.Fv, **42.79.–e**, 68.35.Ct, 68.35.Fx, 68.47.De, 68.55.A, 68.65.Ac, **81.15.–z**

Beryllium-based multilayer X-ray optics

V N Polkovnikov, N N Salashchenko, M V Svechnikov, N I Chkhalo

DOI: https://doi.org/10.3367/UFNe.2019.05.038623

Contents

1.	**Introduction**	**83**
2.	**Calculation of reflection properties of beryllium-containing multilayer mirrors in the vacuum ultraviolet region**	**85**
3.	**Technique of X-ray multilayer mirror deposition**	**85**
4.	**Methods for studying internal structure and reflectivity**	**87**
	4.1 Hard X-ray diffractometry; 4.2 Soft X-ray and vacuum ultraviolet reflectometry; 4.3 Transmission electron microscopy; 4.4 Secondary ion mass spectrometry	
5.	**Internal structure and reflection characteristics of beryllium-containing multilayer X-ray mirrors**	**90**
	5.1 Multilayer X-ray mirrors for photolithography; 5.2 Multilayer X-ray mirrors for studying the solar corona in the vacuum ultraviolet region	
6.	**Conclusions**	**94**
	References	**94**

Abstract. The article provides a review of the current state of affairs in the field of physics and technology of multilayer beryllium-containing mirrors intended for projection lithography and solar corona studies in the extreme ultraviolet (EUV) region. The methods of synthesizing and studying beryllium-containing multilayer mirrors are described. The results of recent studies on the internal structure and EUV reflection coefficients are given for Mo/Be, Mo/Si, Be/Al, and Be/Mg multilayer mirrors. The effect of Si and Be interlayers on the reflectivity is explained. Avenues for further research on beryllium-containing mirrors are discussed.

Keywords: multilayer X-ray mirror, X-ray projection photolithography, microscopy, astronomy, spectroscopy, reflectometry, magnetron sputtering, nanofilm synthesis, beryllium, reflectance, interlayer

1. Introduction

Multilayer X-ray mirrors (MXMs) that provide high reflection coefficients in a broad wavelength range ($10^{-2}-10^{2}$ nm) enjoy wide application in a variety of science, engineering, and technology areas. So broad a dissemination of MXMs is attributable to their several capabilities unattainable with other optical elements. In particular, being Bragg-type reflectors, MXMs, unlike crystals, can be fabricated with almost any period (the analogue of the spacing between crystal planes), thereby spanning a broad (four orders of magnitude) wavelength range. MXMs can be deposited on substrates of arbitrary surface shapes, thereby providing the collimation and focusing of X-ray radiation and imaging [1, 2]. The substrates may vary in size from several millimeters to 1 m [3, 4]. Use can be made of different substrate materials, including those with a high thermal conductivity, making it possible to employ MXMs under exposure to extreme incident radiation fluxes [5–8].

Another special feature of MXMs is the capability to control the spectral reflection band over wide limits. This is significant, because some problems require maximizing the number of reflected photons produced by a source, while others call for reflecting one selected spectral line and suppressing the immediate surroundings. With periodic MXMs, this is achieved by selecting material pairs and/or varying the fraction of the strongly absorbing material in the period. For instance, to narrow the spectral reflection band, materials with a lower absorption and a lower optical contrast at the interfaces are selected (see, for instance, Refs [9–13]). In some cases, it suffices to decrease the fraction of the strongly absorbing substance in the MXM period [13, 14]. To broaden the spectral reflection band, conversely, use is made of material pairs with a high optical contrast at the interfaces, and/or the fraction of the strongly absorbing substance in the MXM period is increased. However, a significant broadening of the mirror reflection band may be achieved by using aperiodic MXMs (all layer thicknesses in the structure are different) [15–19] or stack systems (the MXM consists of several periodic blocks with different periods) [20–22]. These MXMs also permit relaying femto- and attosecond beams of electromagnetic radiation without time spreading of the wave packet or even shortening the pulse duration [23–25].

Free-standing, substrate-free, periodic MXMs make it possible to split X-ray beams as well as to change and analyze their polarization state [26, 27].

New tasks call for constant improvement in X-ray optical MXM characteristics. In particular, new missions presently being developed to study solar corona in the vacuum

V N Polkovnikov [(*)], **N N Salashchenko, M V Svechnikov, N I Chkhalo**
Institute for Physics of Microstructures, Russian Academy of Sciences, ul. Ul'yanova 46, 603950 Nizhny Novgorod, Russian Federation
E-mail: [(*)]polkovnikov@ipmras.ru

Received 18 July 2019
Uspekhi Fizicheskikh Nauk **190** (1) 92 – 106 (2020)
Translated by E N Ragozin; edited by V L Derbov

ultraviolet (VUV) spectrum call for simultaneous improvement in the temporal and spatial resolution of solar telescopes [28]. These goals may be achieved by increasing the diameter of the primary telescope mirror as well as by improving the reflectivity and spectral selectivity of reflective coatings.

Most important for lithographic applications is the reflectivity improvement in traditional Mo/Si mirrors at a wavelength of 13.5 nm and the quest for new multilayer mirror compositions to provide a high reflectivity at wavelengths shorter than 13.5 nm [29–33]. This task is critically important for the development of next-generation lithography. In view of the large size of the microelectronic market and the large number of mirrors (up to 12) in the optical lithographic system, an increase in MXM reflectivity by only 1–1.5% results in a significant economic effect.

X-ray microscopy in the 'water transparency window,' at wavelengths of 2.3–4.4 nm, offers truly unique opportunities for microbiology [34–36]. Since the periods of the multilayer mirrors of a microscope are about 1.5 nm and, accordingly, the individual layer thicknesses are about 0.7–0.8 nm and their total number amounts to 1000, the problem of achieving high MXM reflectivities in this range is presently very intricate.

Apart from X-ray optical MXM characteristics, of importance for several applications is the long-term stability of the characteristics. For instance, for space applications, the in-orbit service life must last for at least seven years. In this case, the time required for different tests and storage, including storage in hangars, which amounts to several years, as a rule, must also be included. Account should also be taken of the broad temperature range, both prior to telescope deployment and in the course of its operation.

The problem of thermal MXM stability has recently become topical in connection with the advent of ultrahigh-power radiation sources — free-electron lasers and third- and fourth-generation synchrotrons.

The above list of requirements imposed on multilayer X-ray mirrors testifies to the necessity of a complex long-term approach to the introduction of new-composition MXMs.

To date, the majority of materials possessing promising (from the standpoint of X-ray optics) values of optical constants and allowing their thin-film vacuum deposition has been adequately studied, and the reflectivities of MXMs that use these materials have practically reached their technological limit. Owing to its weak absorption and low scattering power in the X-ray range, beryllium is the main material of choice for the low-absorption layers in MXMs. However, beryllium has not enjoyed wide use in multilayer X-ray optics. In our view, this is due to the fact that beryllium has primarily been regarded only as a low-absorption and low-scattering material. The properties of Ti/Be mirrors in the VUV region were investigated in Refs [7, 37, 38]. However, due to a high interlayer roughness, the experimentally obtained reflectivities turned out to be lower than for Mo/Si mirrors. As shown in Ref. [39], W/Be MXMs offered an advantage over W/C MXM in the X-ray range, but W/Si- and W/B_4C MXMs, which appeared more recently, turned out to be even better.

The late 1990s and the early 2000s saw a surge of interest in beryllium-containing mirrors related to the wavelength choice for VUV lithography [29, 40–42]. A record high normal-incidence reflectivity of 70.2% was obtained at a wavelength of 11.3 nm in Ref. [43]. According to simulations, Ru/Be MXMs possess an even higher reflectivity and a broader spectral width of the reflection peak. However, practice showed that their experimental reflectivities were lower than for Mo/Be MXMs [43]. In the 'lithographic contest' between beryllium (wavelength: 11.3 nm) and silicon ($\lambda = 13.5$ nm) optics, it was the silicon one which won. The reason was as follows. Although Mo/Si MXMs showed a slightly lower (at that time) reflectivity, their spectral transmission band was broader and the tin radiation source efficiency turned out to be somewhat higher, with the combined effect that the productivity of the lithography tool at a wavelength of 13.5 nm was higher than that at a wavelength of 11.3 nm. Furthermore, work with silicon optics is much simpler, since there are no sanitary restrictions, which are unavoidable when working with beryllium. That is why the interest in beryllium largely waned.

Nevertheless, apart from demonstrating high reflectance of Mo/Be mirrors, one of the most important outcomes of these studies was a detailed measurement of the optical constants of beryllium in the wavelength range of 40–250 nm [44].

The Institute for Physics of Microstructures (IPM), RAS, is one of the leaders in the area of multilayer X-ray optics. Its activities involve practically all aspects: from the physics and fabrication technology of multilayer mirrors to their application in scientific research [45]. A laboratory for the deposition of beryllium-containing mirrors was set up at IPM RAS in 2014. All safety requirements for work with this material were complied with. The reason for resuming work on beryllium was as follows. First, with the progress of work on VUV lithography, certain limitations of this method showed up. In particular, a rapid start was made on 'after 13.5-nm' shorter-wavelength lithography. Proposed in Ref. [46] was a feasibility study on the use of a 6.6–7-nm spectral region, where the simulated reflectivity of La/B mirrors ranges up to 80%. The study encompassed all key aspects of lithography: multilayer optics, radiation sources, and photoresists [31, 32, 47–51]. However, as shown in Ref. [52], despite the progress along all these lines, the $\lambda = 6.7$-nm lithography is an order of magnitude below the $\lambda = 13.5$-nm lithography in productivity. Furthermore, proceeding from new data on the efficiency of xenon-based sources in the vicinity of $\lambda = 11$ nm and the simulation of Mo/Be, Ru/Be, and Rh/Sr mirror reflectances, the 11.2-nm (Be-based optics) and 10.8-nm (Sr-based optics) wavelengths were shown to be the most realistic alternatives to $\lambda = 13.5$ nm. The prospect of increasing the Mo/Be, Ru/Be, and Rh/Srr mirror reflectivities was linked with the development of 'interface engineering' technology, which made it possible to improve (in some cases significantly) the quality of interlayer boundaries [12, 53–55].

Second, the work on beryllium-containing mirrors was motivated by the need to raise the peak reflectivity and spectral selectivity of MXMs for solar corona research in the VUV region. An analysis of the optical constants of beryllium in the VUV performed at that time showed that one might expect a significant improvement in MXM characteristics if beryllium were used not as a low-absorption and low-scattering material (spacer), as it had always been treated, but, conversely, as a strongly scattering material combined with Al and Mg.

This paper is concerned with the method of making and studying beryllium-containing multilayer mirrors. We outline the results of investigations of the internal structure and VUV reflectivity of Mo/Be, Mo/Si, Be/Al, and Be/Mg multilayer mirrors. Also considered is the effect of Si and Be interlayers

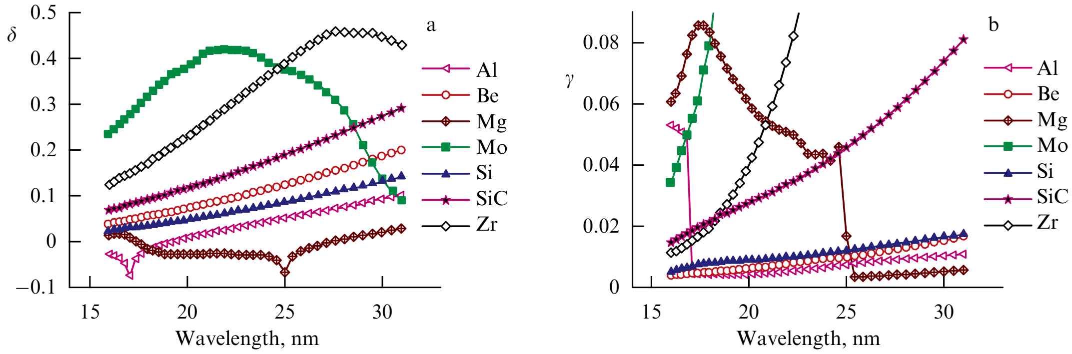

Figure 1. (Color online.) Real (a) and imaginary (b) components of the dispersive part of the permittivity of materials employed for VUV-range MXMs shown in comparison to those for a beryllium MXM.

on the reflectivities. We discuss avenues for further research on beryllium-containing mirrors.

2. Calculation of reflection properties of beryllium-containing multilayer mirrors in the vacuum ultraviolet region

The VUV region is characterized by strong absorption, which limits the choice of weakly and strongly absorbing materials. For a weakly absorbing material, use is made of beryllium (wavelength range: 11.1–12.4 nm), silicon ($\lambda = 12.4-17$ nm), aluminum ($\lambda = 17.1-60$ nm), and magnesium ($\lambda = 25-60$ nm). For strongly scattering materials, use is made of molybdenum ($\lambda = 10-60$ nm) [56–59] and zirconium ($\lambda = 17-20$ nm) [60]. MXMs based on these materials possess rather high reflectivities. With oxidation protection, the X-ray optical characteristics of these MXMs are highly stable (see, for instance, Refs [61, 62]). While molybdenum is the material of choice for 11.1–13.5-nm wavelength lithography (with the exception of the $\lambda \approx 11$-nm domain, where ruthenium rivals molybdenum), which calls for maximizing the peak and integral reflectivities, the problem of selecting a strongly absorbing (scattering) material in the $\lambda > 17$-nm domain is quite acute. This is because the $\lambda > 17$-nm domain is of interest for the study of solar corona and high-temperature plasmas. These objects are characterized by a large number of narrow spectral lines [13]. In this case, researchers face the task of extracting the line of interest and minimizing the contribution of neighboring lines.

Because the absorption and the interfacial optical contrast are high, the extinction depth in Mo- and Zr-containing MXMs is short. As a consequence, the spectral reflection band is broad. Therefore, recent years have seen an active quest for a scattering material capable of providing both a high peak reflectivity and a narrow spectral transmission band. Certain success was achieved with the use of Si-based [13] and SiC-based [62–65] MXMs. Attempts to significantly improve the spectral selectivity with the use of these mirrors met with success. However, because of an insufficiently high contrast at the interfaces with Al and Mg, their reflectivities turned out to be lower than for Mo- and Zr-based mirrors.

The real and imaginary components of the dispersive part of the permittivity of materials employed for VUV-range MXMs are depicted in Fig. 1 in comparison with those for beryllium. The optical constants were borrowed from the CXRO (Center for X-Ray Optics) database (http://henke.lbl.gov/optical_constants/) [66]. With reference to Fig. 1, Be exhibits a lower absorption and a higher optical contrast than does Si, which testifies to the possibility of achieving a higher reflectivity for a comparable spectral selectivity. By comparing Be and SiC, one can see that the optical contrast for SiC is higher than for Be, but the absorption is much higher than for Be. In this case, one would expect, at the very least, comparable reflectivities for a higher spectral selectivity.

The simulated spectral reflectivities in the vicinity of $\lambda = 17.5$ nm and in the vicinity of the 30.4-nm line of HeII are plotted in Fig. 2 for the MXMs presently employed in the VUV range, in comparison with those for Be/Al and Be/Mg mirrors. As is clear from the figure, numerical calculations bear out the above qualitative reasoning. Beryllium is the scattering material of choice, providing simultaneously a high reflectivity and a high spectral selectivity.

3. Technique of X-ray multilayer mirror deposition

To synthesize beryllium-containing multilayer mirrors, at IPM RAS a dedicated laboratory was set up and equipped with ventilation and exhaust systems with several cleaning stages. The vacuum line of the technological facilities was also equipped with a filtration system. The beryllium content in the air is regularly monitored, including that in the immediate vicinity of the open vacuum chamber. In accordance with safety regulations and instructions, all consumables are utilized, including the operator's protection means and workwear.

The laboratory accommodates two magnetron sputtering facilities, which differ by the number of magnetron sources (magnetrons): four in one facility and six in the other one. The number of magnetrons determines the maximal number of materials which may be deposited on a substrate in the framework of one technological procedure. Figure 3 shows a schematic diagram and photograph of one magnetron sputtering facility with the ensemble of the corresponding equipment.

The facility comprises a vacuum volume, an evacuation system, magnetrons, substrate rotation devices, power supply units, and process control systems (the last two elements are not shown in Fig. 3). The evacuation system, which consists of a turbomolecular pump with a pump capacity of 2200 l s^{-1} and a backing pump with a capacity of 8.3 l s^{-1}, provides a residual gas pressure at a level of 10^{-5} Pa. The residual pressure is directly related to the number of impurities

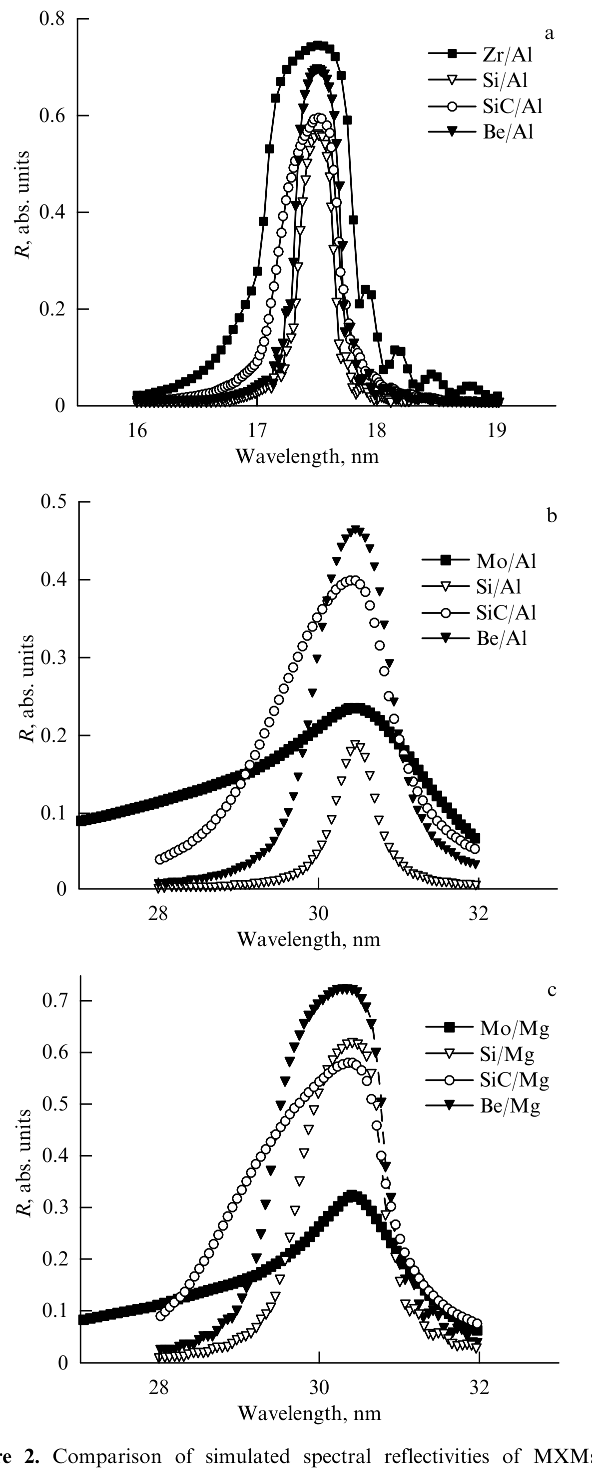

Figure 2. Comparison of simulated spectral reflectivities of MXMs presently employed in the VUV region with those for Be/Al and Be/Mg multilayers: (a) in the vicinity of $\lambda = 17.5$ nm, (b, c) in the vicinity of the 30.4-nm line of HeII.

(primarily oxygen) that find their way into the growing films. As shown experimentally, the oxygen content in an MXM rises significantly when the pressure is one order of magnitude higher than the maximum technologically admissible pressure. The magnetrons (four or six, depending on the specific facility), which are planar-type sources, are accommodated along the perimeter of the chamber bottom. The arched magnetic field promotes the formation of an annular erosion zone on the target surface (inner diameter of the ring: 95 mm; outer diameter: 115 mm).

The sputtered targets are mounted on a conducting layer on the magnetron surface. The target is the cathode in the gas discharge under formation. Conducting targets (metals, silicon doped with boron, etc.) may be sputtered in a DC discharge. Nonconducting targets (boron, silicon nitride, etc.) are sputtered by an rf discharge. The magnetrons are fed by stabilized DC units developed at IPM RAS. These units permit varying the discharge current between 100 and 2000 mA for a voltage from 100 to 500 V. For rf target sputtering, use is made of Balzers units with a frequency of 13.56 MHz. In the course of synthesis, typical values of electric power are in the range between 150 and 250 W. The magnetrons with targets are cooled by a forced water feed by means of a pump.

Magnetic induction on the target surface amounts to $(4-7) \times 10^{-2}$ T (depending on the target thickness, which may range up to 10 mm). The magnetic intensity largely defines the energy of particles that find their way into the substrate. For a low field, the energy is proportional to the voltage applied to the discharge, which in turn results in the diffusion of interlayer interfaces [67]. The parameters of the magnetic field in the magnetrons of the described facilities provide a voltage range of 250–300 V at a working gas pressure (99.998% pure argon) of $(2-3) \times 10^{-2}$ Pa in the vacuum volume. In this case, the characteristic film growth rate is of the order of 0.1–1 nm s^{-1} (depending significantly on the target material).

The technological procedure of synthesis is as follows. A substrate is attached to a rotating disk located above magnetrons, with its working surface downwards. Typical target–substrate distances are equal to 75–80 cm. At shorter distances, the substrate is in the region of discharge and introduces perturbations into it, making the process unstable. At longer distances, the film growth rate is lower (owing to a decrease in sputtered material density).

During disk rotation, the substrate passes above the operating magnetrons. Their number is defined by the mirror composition and may amount to four or six (depending on the technological facility). This permits the layers to be deposited sequentially, one after another. The whole structure period is deposited in one disk revolution. By varying the velocity of substrate passage (the angular velocity of disk rotation) above the magnetrons, it is possible to control the deposited layer thicknesses.

In addition to the disk rotation, the substrate revolves about its axis with a high angular velocity (up to 10 revolutions per second). This provides an angular uniformity to the coating.

Mounted above each magnetron are precision figured apertures to provide requisite uniformity of film thicknesses or a given MXM period distribution over substrate radius. By varying their shape, it is possible to control the flux density distribution of the material delivered to the substrate. The precision of controlling the period distribution over the mirror area may be as high as 0.2% of the period.

The stringent specifications for the periodicity of mirror coatings imposes rigid requirements on the parameter stability of the technological process, like the working gas pressure in the chamber, electrical power in the magnetrons, and speed of substrate passage above the magnetrons. The fluctuations or drift of these parameters affect the growing layer thicknesses. In the first approximation, this dependence may be considered linear. For instance, a 1% variation in the electrical power in the magnetron will result in a similar

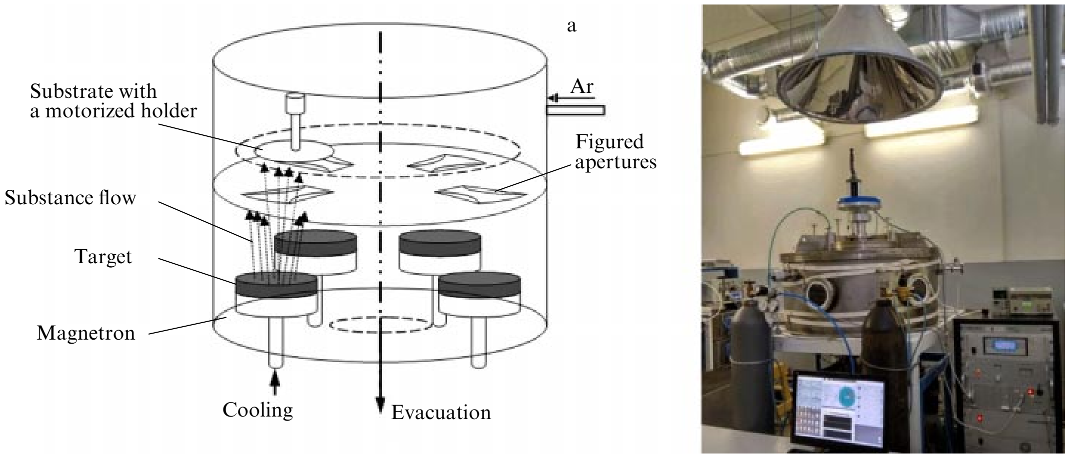

Figure 3. Schematic diagram (a) and photograph (b) of a magnetron sputtering facility with the ensemble of the corresponding equipment.

variation in the growing layer thickness of a given material. The requirement for the MXM period maintenance accuracy may be estimated as $\Delta d < d/N$, where Δd is the period fluctuation amplitude, d is the structure period, and N is the number of reflecting periods. For instance, for a normal-incidence Cr/Sc MXM [68] designed for a wavelength of 3.12 nm, the period $d \approx 1.56$ nm, the number of periods $N = 400$, and the admissible spread in periods with structure depth is $\Delta d < 0.004$ nm (or less than 0.25%).

The task of stabilizing the technological process parameter is solved with a hardware-software tandem based on a commercial i-8431 PC-compatible controller. A personal computer is used to monitor and log the process parameters. Furthermore, during the synthesis, it is necessary to take into account the possible variations in conditions, in particular, in the residual gas composition, the target surface state, and the temperature of the fittings surrounding the magnetron. To provide stability of the process parameters, it is necessary to secure stationary conditions in the synthesis chamber prior to the deposition of a multilayer coating.

As a rule, stationary conditions in the synthesis chamber set in during the long (about 1 hour) idle (without material deposition on a substrate) magnetron operation. In the course of idle work, external conditions become balanced, the upper, oxidized, target layer is etched, the temperature of the target and fittings reaches its stationary level, and the stationary state is reached in the atmosphere, which consists of the residual and working gases.

All samples described in this paper were deposited on superpolished silicon plates with an effective rms roughness of about 0.3 nm in the spatial frequency range of 0.02–60 μm^{-1}. The roughness was measured on a special test bench using the method described in Refs [69, 70].

4. Methods for studying internal structure and reflectivity

Since individual MXM-constituting films are thin (of the order of $\lambda/4$), the mirror reflectivities are to the utmost extent determined by the state of interlayer domains and roughness. In effect, the physics and technology of multilayer X-ray mirrors is the physics and technology of interlayer boundaries (interfaces). That is why improving the X-ray optical MXM characteristics is directly related to the study of internal MXM structure, primarily the thickness and profile of the interlayer regions. The sensitivity of methods should lie at an angstrom or subangstrom level.

4.1 Hard X-ray diffractometry

One of the standard techniques widely used to monitor layered nanostructures involves reflectometric measurements. The rapidity of measurements with laboratory diffractometers and the sensitivity of the method to film thickness variations of about 1 Å underlie the wide use of these instruments. Reflectometric measurements are nondestructive and do not require special sample preparation, and measurements in the hard X-ray (HXR) range may be performed in the air, which simplifies the measurement procedure still further. As a rule, laboratory reflectometers operate on the copper $K_{\alpha 1}$ line with a wavelength of 0.154 nm, and the source intensity permits measuring the reflectivity to a value of about 10^{-6}. In some cases, the dynamic range of the diffractometer may range up to eight orders of magnitude [71], which is comparable to the capabilities of synchrotron stations. The reflectivity of an interlayer boundary depends heavily on the state of the interface. This circumstance, in combination with the wide dynamic range, offers a unique set of capabilities for studying the state of interfaces and the processes that occur there in the growth and operation of the structure. Figure 4 depicts the reflectivity curves for a periodic Mo/Be mirror prior to and after annealing.

Reflectometric diagnostics is an indirect method: data interpretation depends greatly on the structure model employed to solve the inverse problem [72]. The main method of reflectometric curve analysis involves construction of a model based on a priori information and general physical considerations, as well as numerical fitting of parameters like layer thicknesses and densities, effective roughness, and interfacial transition layers [73]. The interface model is strictly defined in this case. Of course, this approach is legitimate only when the a priori model provides an adequate description of the structure. Under this formulation of the problem, the discovery of new features in substance distribution and the investigation of poorly known ones is difficult, if at all possible.

For MXMs, representation in the form of a simple model is the traditional and, in a sense, natural approach: the reflectivity of a periodic binary structure with sharp boundaries may be found in an analytical form [74, 75]. When the

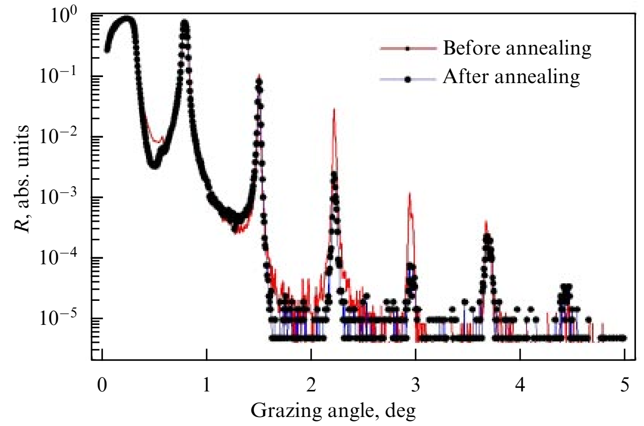

Figure 4. (Color online.) Reflection curves for a periodic Mo/Be mirror prior to and after annealing in the air for 2 hours at a temperature of 350 °C. Wavelength: 0.154 nm.

diffuse boundary model is employed, in several cases it is possible to use modified reflection coefficients for every interface. The best known corrections are the Névot–Croce and Debye–Waller factors [76], which apply to the transition layer in the form of error function erf(x). Modifying factors for other kinds of transition layers may also be found [77]. The use of modified reflectivities instead of the Fresnel ones permits the use of an analytical expression to calculate and optimize periodic MXMs.

Although the reflectivity is sensitive to the thickness and shape of the interlayer interfaces, reflectometry does not permit separating the contributions of the interpenetration of the layer materials and roughness. In this case, one has to resort to the technique of small-angle HXR scattering by the sample roughness. The height and statistics of the roughness correspond to the intensity and angular distribution of the scattered radiation, while the interlayer correlation in interference structures (and MXMs are precisely such structures) results in constructive or destructive interference of the scattered radiation [78, 79]. Due to the interference, non-specular, so-called quasi-Bragg, resonances are formed in MXMs. Such a resonance is exemplified in Fig. 5b, where it is seen at an angle of 1.5° from the specular direction. From the width, height, and angular position of the quasi-Bragg peaks it is possible to draw a conclusion about the height and in-depth correlation length of the spatial harmonic of the roughness.

4.2 Soft X-ray and vacuum ultraviolet reflectometry

While HXR reflectometry is widely used to monitor layered nanostructures in various areas of science and technology, reflectivity measurements in the soft X-ray (SXR) and VUV regions are much more a niche-like technique, which is most often employed for characterizing X-ray optical elements. These measurements are carried out mostly at working wavelengths. Therefore, not only are they a source of auxiliary information for the subsequent numerical reconstruction of the structure, but they are also a method of certifying coatings and obtaining final information about the performance of X-ray optical elements.

Measurements in the said spectral region are performed in a vacuum chamber, and the intensity of SXR and VUV sources is far lower than that in the HXR domain. Several different types of laboratory reflectometers are used at IPM RAS for the prompt metrology of deposited mirrors. A reflectometer of the first type is based on an RSM-500 spectrometer-monochromator. The radiation source is an X-ray tube with replaceable targets, which permits spanning the wavelength range of 0.9–25 nm [80]. Another reflectometer based on an LHT-30 monochromator with a toroidal grating makes use of a gas-discharge source and permits measurements to be made in the wavelength range of 30–200 nm. A third reflectometer with a Czerny–Turner spectrometer and a broadband laser-plasma source permits measurements to be made in the wavelength range of 5–50 nm using a continuous spectrum, which is critically important in the certification of broadband aperiodic mirrors [82]. Laboratory data are regularly compared with precision data obtained on the Optics Beamline channel of the BESSY-2 synchrotron (Berliner Elektronenspeicherring-Gesellschaft für Synchrotronstrahlung, Berlin) [83, 84], one of world's metrology centers. Figure 6 exemplifies the reflectometric curves of the same sample obtained at IPM RAS and BESSY-2.

4.3 Transmission electron microscopy

There is no way to unambiguously reconstruct the structure of interlayer interfaces from X-ray reflectometry data. To do this calls for additional information. The electron microscopy of the transverse cuts of multilayer structures provides a way to obtain this information. In particular, it permits a comparison of the interfaces in one structure and makes it possible to unambiguously determine which of the interfaces is sharper and which is more diffuse. With High-Resolution Transmission Electron Microscopy (HRTEM), the spatial resolution reaches subnanometer values.

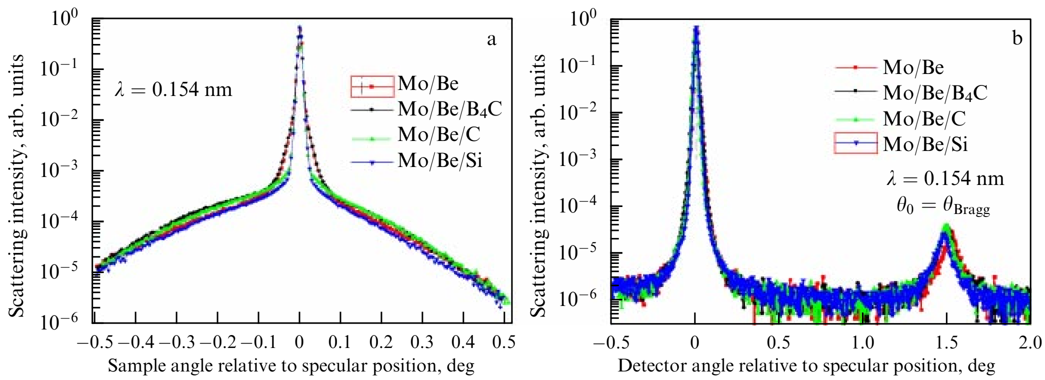

Figure 5. (Color online.) (a) Scattering curves under sample rocking near the specular reflection (first Bragg peak) for periodic Mo/Be MXMs. (b) Result of detector scanning near the specular direction and the quasi-Bragg peak.

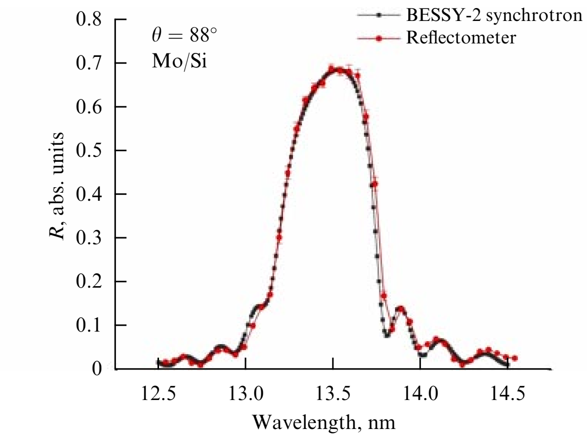

Figure 6. (Color online.) Spectral dependence of the reflectivity of an Mo/Si mirror measured with a laboratory reflectometer and the BESSY-2 synchrotron. The grazing angle measured from the surface is equal to 88°.

The preparation of samples for electron microscopy is rather complicated, unlike their preparation for X-ray techniques. It begins with cutting out lamellas using focused Ga^+ ion beams with an energy of 30 kV. The resultant transverse 1–2-μm thick microscopic sections are not suited to direct analysis by transmission microscopy. That is why a focused 30-kV Ga^+ ion beam is additionally used to etch regions in lamellas to a thickness of 50–150 nm [85]. Under this etching a disturbed layer forms, which precludes obtaining high-quality high-resolution microphotographs. Furthermore, if a lamella etched by high-energy ions is thin, it will consist entirely of the disturbed layer and there will be practically no way to extract qualitative or quantitative information. That is why the lamellas were additionally etched by Ar^+ ions with an energy of 300 eV. The samples thus prepared were investigated by transmission electron microscopy techniques [86, 87]. Figure 7 shows photographs of the microscopic sections of four beryllium-based MXMs.

Apart from the information about interfaces in a sample, the electron diffraction pattern bears information about the MXM period and the degree of crystallicity of the material layers.

4.4 Secondary ion mass spectrometry

Secondary ion mass spectrometry (SIMS) does not possess an angstrom-level resolution in depth and does not yield exact densities of the chemical elements in the layers of a multilayer structure but provides only estimates of them. However, recent years have seen a progressively wider use of SIMS for the study of the internal MXM structure [88–90]. In some cases, due to improvement in the algorithms of density profile reconstruction from SIMS data, it is possible to reveal the asymmetry of elemental distribution within a layer. In particular, the authors of Ref. [91] were able to explain the mechanism of the effect of thin carbon barrier layers in La/B_4C MXMs on the observed increase in the reflectivity of these mirrors in the vicinity of $\lambda = 6.7$ nm [51]. As shown in Ref. [92], in Be/Al MXMs with silicon interlayers, the transition regions were thinner and the Al and Be modulation depths were higher. The measurement data correlate nicely with X-ray reflectivity data. In Ref. [93], it was solely the use of the SIMS technique that made it possible to explain the approximately 1% increase observed in Mo/Be MXM reflectivity at a wavelength of 11.4 nm with vacuum annealing for 1 h and its subsequent lowering with an increase in annealing time. The measured oxygen density profiles in the layers (Fig. 8) suggested that the density maxima in the prepared samples fall on beryllium films. After annealing, the oxygen modulation becomes lower, testifying to a partial transition of oxygen to molybdenum films. Under Bragg resonance conditions, the antinode of the standing wave falls on the beryllium films, and therefore the average absorption in the MXM decreases, resulting in the increase in reflectivity. The lowering of reflectivity with increasing annealing time is attributed to an increase in the oxidation depth of the upper MXM layers and the consequential additional absorption. In general, protective (antioxidative) layers play an important role in MXM technology, and

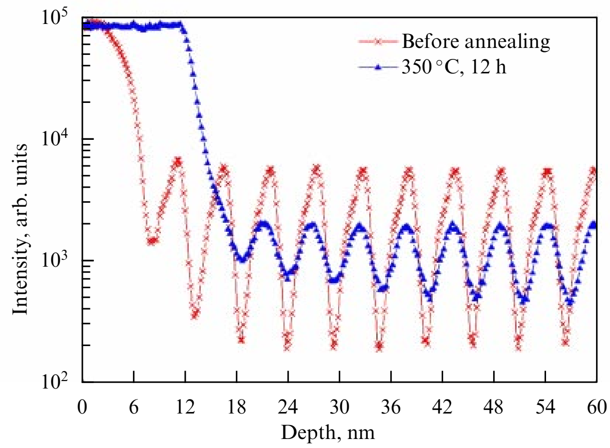

Figure 8. Oxygen distribution in an Mo/Be MXM prior to and after annealing for 12 h.

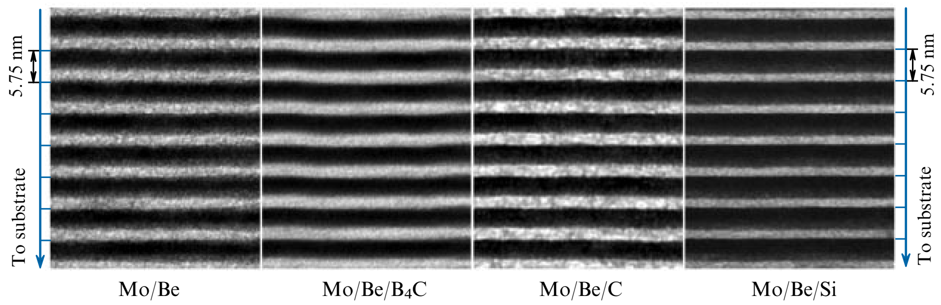

Figure 7. HRTEM images of the microscopic sections of beryllium-based MXMs. Bright domains correspond to the transparent material (Be) and the dark ones correspond to the opaque one (Mo).

especially so in the VUV, where oxygen-induced absorption is strong. The frequently used method of reflectivity curve fitting always yields ambiguous solutions, and the SIMS investigation of the oxygen distribution with depth may therefore yield additional information, making it possible to correct the model when fitting reflectivity curves.

The SIMS technique may be extremely helpful in the study of different kinetic processes related to the migration of atoms in multilayer film structures. For instance, observed in Ref. [94] was a complete solution of boron from the protective upper B_4C layer in the interior of a thin-film structure under annealing. In our opinion, researchers working in the area of multilayer X-ray and neutron mirrors have not yet fully recognized the broad capabilities of SIMS and, accordingly, do not place due emphasis on this promising technique of multilayer thin-film structure diagnostics.

5. Internal structure and reflection characteristics of beryllium-containing multilayer X-ray mirrors

5.1 Multilayer X-ray mirrors for photolithography

As noted in the Introduction, of paramount importance for lithographic applications are the magnitude of the reflectivity and the spectral bandwidth of an MXM. For optimal values of these parameters, it is possible to maximize the utilization efficiency of the useful source radiation, since the Sn and Xe emission bandwidths exceed the bandwidth of the optical lithographic system [49, 95–97]. In a multimirror system (there are up to 12 mirrors in a modern VUV lithographic system) [98], the increase in reflectivity by only 1.5%, say from 70% to 71.5%, results in an almost 30% increase in the productivity of the lithographic process. In view of the production scale of microelectronics, this is a breakthrough achievement.

We have studied the feasibility of improving the Mo/Be mirror reflectivity. In the course of investigations, a reflectivity of 70.25% [87] was obtained at a wavelength of 11.3 nm and an off-normal incidence angle of 6°, which is an exact reproduction of the earlier results published in Ref. [43]. Our research showed that the main reason for the low reflectivity, in comparison with a theoretical figure of 76%, is the diffusiveness of boundaries, the Mo-on-Be boundary being the worst one.

Similar results were obtained for Ru/Be MXMs: the reflectivity turned out to be appreciably lower than 70%.

To solve this problem, we studied the possibility of improving the boundaries with thin interlayers of C, B_4C, and Si, which proved to be helpful in other systems [53, 54, 99, 100]. Since the worst boundary was the Mo-on-Be one, the interlayers were deposited above Be layers. Figure 9 shows the results of fitting the experimental reflectivity curves for samples with and without the interlayers. Shown in the left part of Fig. 9 are the angular dependences of the reflectivity at a wavelength of 0.154 nm and in the central part at wavelengths of 11.3–11.4 nm. Shown in the right part of Fig. 9 are the spectral dependences of the reflectivity near $\lambda = 11.4$ nm measured at an incidence angle of 2° from the normal. Red curves with symbols stand for experimental data and the blue curves show the fitting data. The MXM parameters reconstructed from these data are collected in Table 1.

As is clear from Table 1 and Figs 9a, 9b, 9d, 9g, 9h, 9j, and 9k, the interlayers only impaired the VUV reflectivities of Mo/Be MXMs. In the case of B_4C and C interlayers, this was associated with the broadening of transition regions due to an increase in interlayer roughness rather than due to diffusion of the materials, as suggested by the data of the investigations of diffuse X-ray scattering and atomic force microscopy of the sample surfaces. A smoothing of the Be-on-Mo boundary is observed with the silicon interlayer. The lowering of reflectivity near $\lambda = 11.4$ nm is due to the strong absorption in silicon behind its L absorption edge, $\lambda = 12.4$ nm. The results of this investigation are minutely set forth in Ref. [87]. Although attempts to increase the VUV reflectivity of Mo/Be MXMs with the use of interlayers did not meet with success, the smoothing of boundaries due to Si interlayers became an important result of the investigation discussed below.

An investigation of the effect of vacuum annealing on Mo/Be mirrors showed that some improvement of reflectivity was possible. The effect is unstable due to the concurrent oxidation of the upper layers. In addition, as is clear from the SIMS data, the upper MXM period is partly oxidized, which lowers the mirror reflectivity in view of the double transmission of the wave in the reflection. To solve this problem, we synthesized Mo/Be MXMs with a protective Ru capping layer. The layer thickness, which was selected so as to maximize the VUV reflectivity, was equal to 1.8 nm. Figure 10 depicts the spectral dependence of the VUV reflectivity of this

Table 1. Main characteristics of samples obtained by fitting X-ray reflection curves.*

Sample	Composition	$\langle d \rangle$, nm	$\langle h(\mathrm{M}) \rangle$, nm	Thickness of transition layers, nm	$\Delta\lambda_{1/2}$, nm	$\lambda_{\mathrm{peak}}(88°)$, nm	R, %
D364	Mo/Be	5.67	$h(\mathrm{Be}) = 3.44$ $h(\mathrm{Mo}) = 2.23$	Mo-on-Be = 0.67 Be-on-Mo = 0.33	0.26	11.31	69.7
D366	Mo/Be/B_4C	5.75	$h(\mathrm{B_4C}) = 0.36$ $h(\mathrm{Be}) = 3.34$ $h(\mathrm{Mo}) = 2.05$	Mo-on-B_4C = 0.74 B_4C-on-Be = 0.77 Be-on-Mo = 0.5	0.29	11.45	67.6
D381	Mo/Be/C	5.78	$h(\mathrm{C}) = 0.39$ $h(\mathrm{Be}) = 2.95$ $h(\mathrm{Mo}) = 2.44$	Mo-on-C = 0.6 C-on-Be = 0.87 Be-on-Mo = 0.39	0.29	11.45	68.2
D383	Mo/Be/Si	5.85	$h(\mathrm{Si}) = 0.48$ $h(\mathrm{Be}) = 3.04$ $h(\mathrm{Mo}) = 2.33$	Mo-on-Si = 0.72 Si-on-Be = 0.16 Be-on-Mo = 0.28	0.29	11.59	66.5

* $\langle d \rangle$ — average period, $\langle h(\mathrm{M}) \rangle$ — film thickness averaged over all periods.

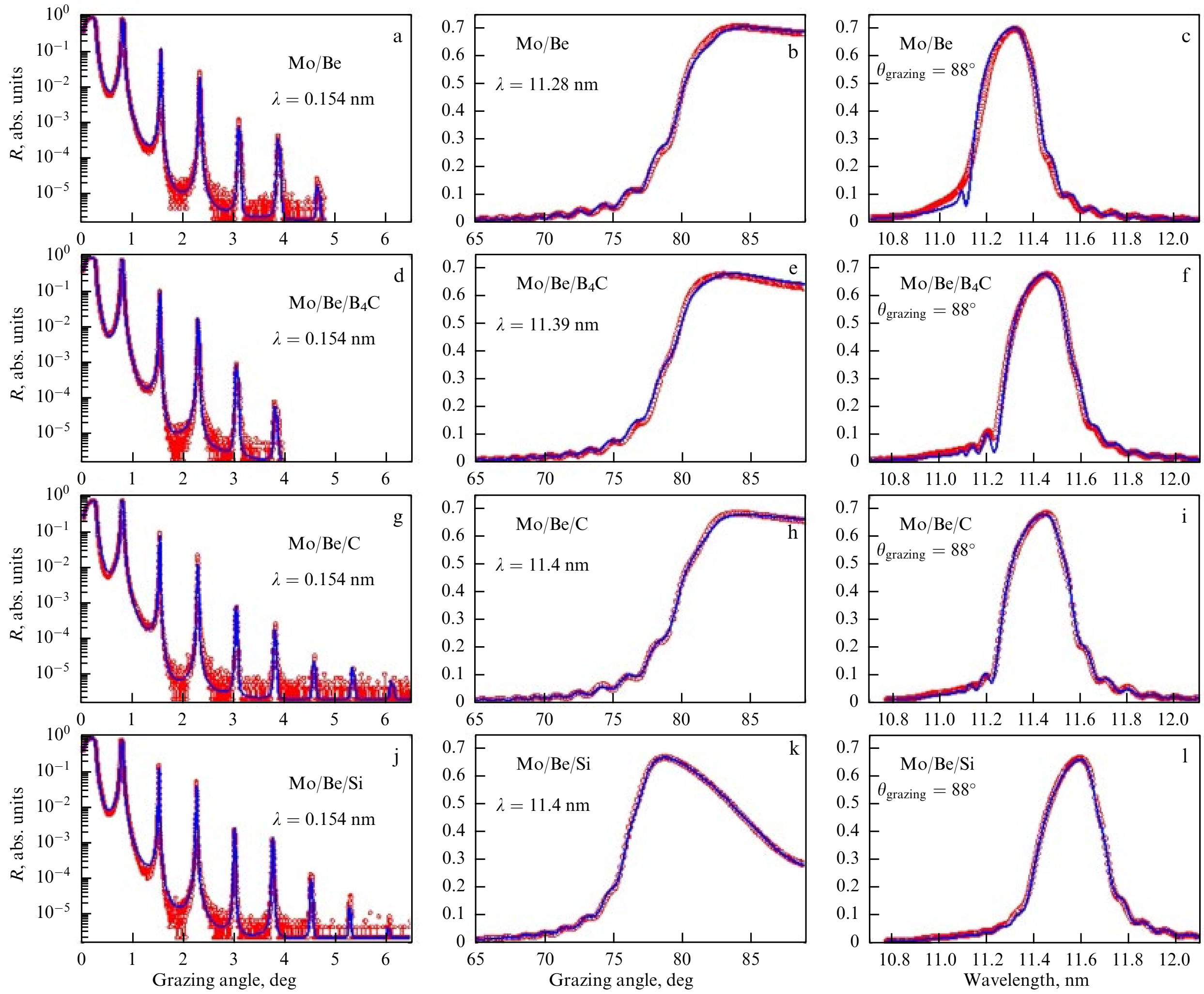

Figure 9. (Color online.) Experimental reflectivities and reflectivities reconstructed from these data. Red curves with symbols stand for experimental data and blue curves represent the result of fitting.

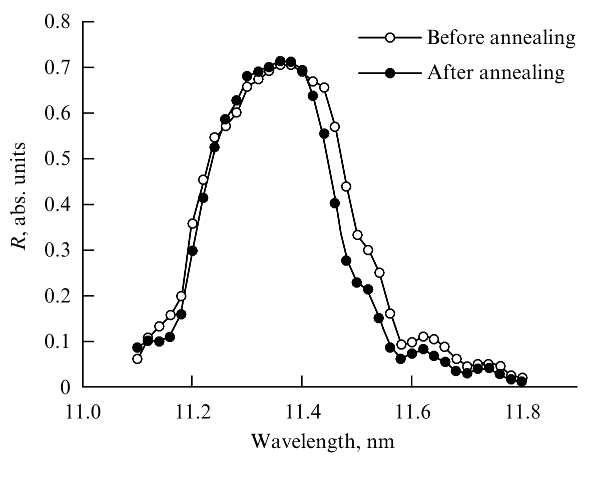

Figure 10. Spectral dependences of the VUV reflectivity of a Mo/Be mirror with a protective Ru layer measured for an off-normal incidence angle of 5° after annealing for 1 h at a temperature of 300 °C.

sample. The off-normal incidence angle was equal to 5°. The measurements were carried out using a reflectometer with a laser-plasma X-ray source and plane-grating monochromator [82]. The spectral width of the probing beam was to 0.03 nm.

As is seen in Fig. 10, the reflectivity of the Mo/Be sample with an Ru protective layer became high and, after annealing, amounted to a record figure $R = 71.2 \pm 0.6\%$ for a half-height width of the reflection curve $\Delta\lambda_{1/2} = 0.32$ nm.

As noted above, among the interesting results is the smoothing of roughness in Mo/Be mirrors with the use of silicon interlayers. Its possible effect on the reflectivities of classical Mo/Si MXMs at a wavelength of 13.5 nm was first considered theoretically in Ref. [101]. As shown there, when use is made of approximately 1.4-nm thick Be interlayers at the Si-on-Mo boundary, one might expect a reflectivity of over 72% in the vicinity of the 13.5-nm wavelength. The importance of this result for lithography lies in the fact that the record reflectivity equal to 70.15% was obtained for Mo/B$_4$C/Mo/B$_4$C MXMs more than 10 years ago [99]. The experiment was performed and the results of investigations were outlined in Ref. [102]. Figure 11 depicts the angular dependences of the reflectivity of Mo/Be/Si MXMs measured at wavelengths of 13.5 and 12.9 nm. At a wavelength of 13.5 nm, the reflectivity $R = 71.89\%$, and at $\lambda = 12.9$ nm $R = 72.83\%$. The half-width of the spectral reflectivity curve at $\lambda = 13.5$ nm was equal to about 0.52 nm, which is still

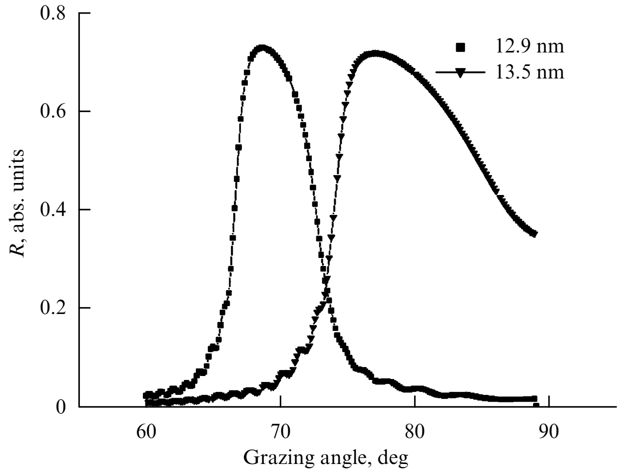

Figure 11. Angular dependences of the reflectivity of Mo/Be/Si MXMs measured at wavelengths of 13.5 and 12.9 nm.

inferior to that for classical Mo/Si mirrors, equal to about 0.53 nm. This difference is due to the fact that the thickness of beryllium interlayers was not optimal in our experiments. Furthermore, there were no barrier B_4C interlayers at the Mo-on-Si boundary, while they were present in the experiment in Ref. [99]. That is why we hope to improve the spectral width of the reflectivity in the Mo/Be/Si/B_4C structure. A preliminary experiment bore out our expectations: the reflectivity curve of the four-component structure broadened to $\Delta\lambda_{1/2}$ =0.535 nm [103].

5.2 Multilayer X-ray mirrors for studying the solar corona in the vacuum ultraviolet region

As noted in Section 4, owing to the weak absorption of beryllium, its use as a scattering material in combination with aluminum and magnesium makes it possible to simultaneously obtain a high reflectivity and a high spectral selectivity in the wavelength range of 17.1–40 nm. Be/Al MXMs were first made in Ref. [100], and their reflection characteristics were studied in the spectral range of 17.1–17.5 nm. Figure 12a shows the measured angular dependence of the reflectivity at a wavelength of 17.14 nm (curve with symbols) and the reflectivity simulated assuming perfect boundaries (solid curve). As is seen in the figure, the reflectivity was about 43% for a theoretically possible value of 66%. The reason lies with the large interlayer roughness, which was found to be equal to $\sigma = 1.3$ nm, according to the fitting of the reflectivity curve at a wavelength of 0.154 nm (Fig. 12b).

To solve this problem, we studied the effect of silicon interlayers on the structure of transition regions and X-ray reflectivities. Among the known efficient interlayers for 'boundary engineering' in MXMs, Si exhibits the lowest absorption in this domain and is therefore a promising material. The interlayers were deposited on different boundaries and their thicknesses were measured. In the course of investigations, it was found that the VUV reflectivities increase on Si deposition at any boundary (or simultaneously on both). However, the reflectivity is maximal when a 0.8–1-nm-thick silicon interlayer is deposited only on one boundary — above a beryllium layer.

Figure 13 depicts the angular dependences of the reflectivities of Be/Si/Al MXMs at wavelengths of 17.14 and 0.154 nm. As is seen in the figure, the VUV reflectivity increased by a factor of almost 1.5, and distant Bragg reflection peaks appeared on the $\lambda = 0.154$-nm curve. The reflectivity increased due to the lowering of interlayer roughness from 1.3 nm to 0.7 nm. This is qualitatively explained by the fact that aluminum films are fine-crystalline in structure at the initial stage of their growth. As the thickness increases, the crystallites increase in size, which results in an increase in film surface roughness. Amorphous silicon interlayers impede the growth of crystallites, because the aluminum film starts to grow on an amorphous surface at each period.

The reflective properties of Be/Si/Al MXMs at a wavelength of 30.4 nm (the HeII line) were studied in Ref. [104]. Figure 14 shows the angular dependences of the reflectivity of a Be/Si/Al sample measured at a wavelength of 30.4 nm immediately after deposition, as well as 8 and 20 months later. One can see from the figure that the reflectivity changed by no more than 2% during 20 months of storage in the air.

The spectral dependence $R(\lambda)$ was measured for the same structure at an off-normal incidence angle of 2°. The measurement results are presented in Fig. 15. The peak reflectivity $R = 34.3\%$ and the spectral selectivity $\Delta\lambda_{1/2} = 1$ nm. The Be/Si/Al MXM excels the structures used by other research groups both in spectral selectivity and in the

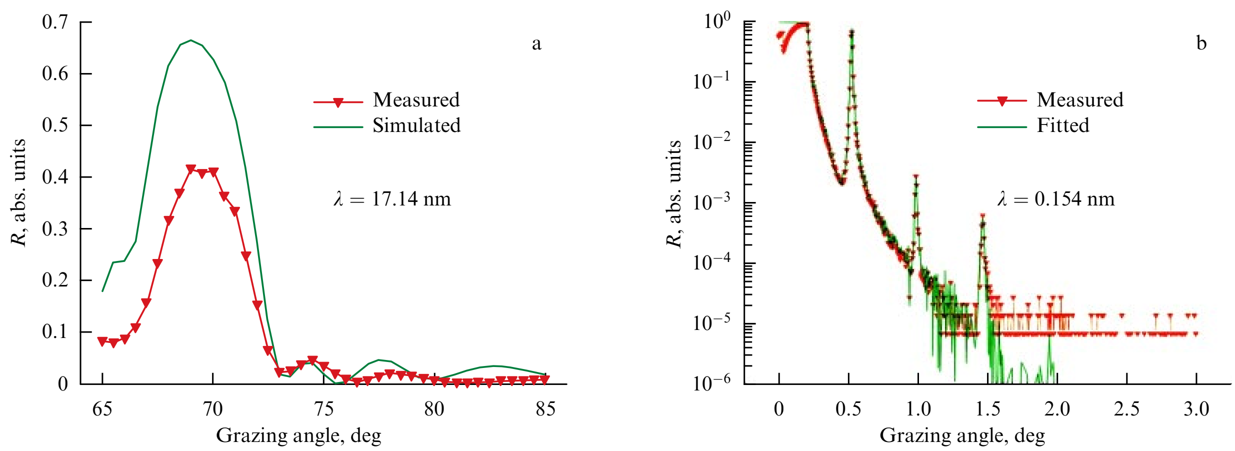

Figure 12. (Color online.) (a) Angular dependences of the Be/Al MXM reflectivity at a wavelength of 17.14 nm: reflectivity simulated assuming perfect boundaries (solid curve) and the measured one (curve with symbols). (b) Measured (curve with symbols) and fitted (solid curve) angular dependences of the reflectivity at a wavelength of 0.154 nm.

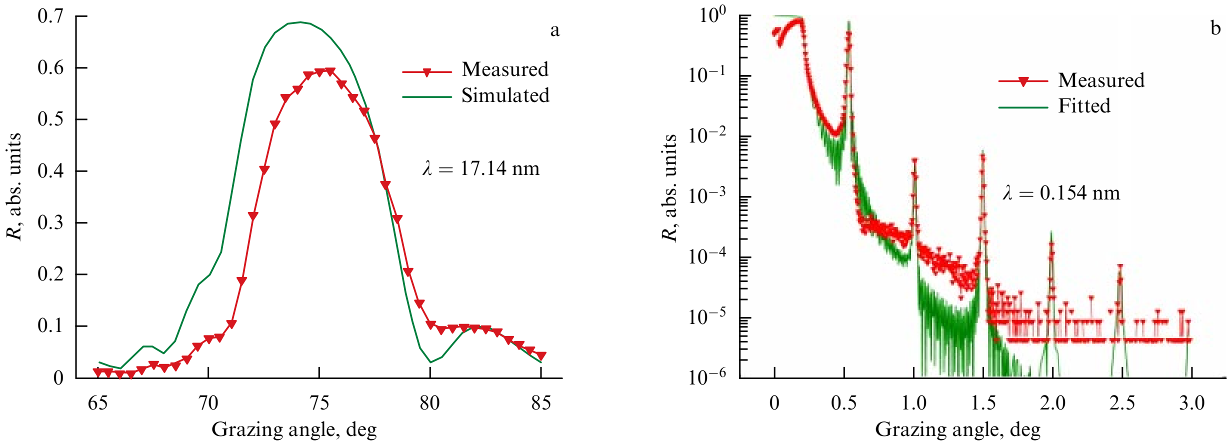

Figure 13. (Color online.) (a) Angular dependences of the reflectivity of Be/Si/Al MXMs at a wavelength of 17.14 nm: simulated assuming perfect boundaries (solid line) and measured (curve with symbols). (b) Measured (curve with symbols) and fitted (solid curve) angular dependences of the reflectivity at a wavelength of 0.154 nm.

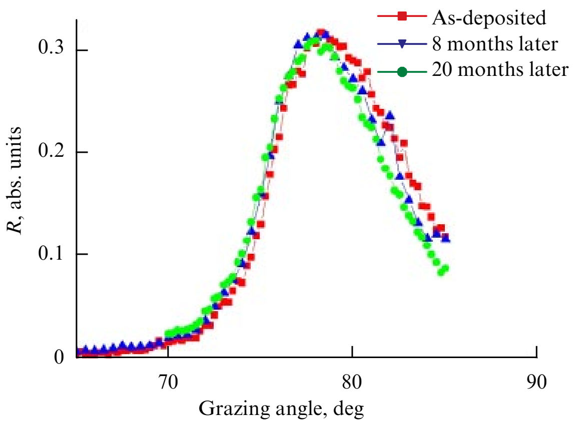

Figure 14. (Color online.) Angular dependences of the reflectivity of a Be/Si/Al mirror measured at a wavelength of 30.4 nm immediately after deposition, as well as 8 and 20 months later.

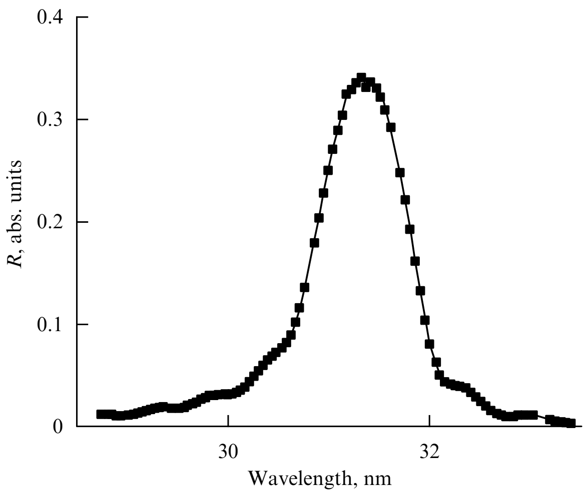

Figure 15. Spectral dependence of the reflectivity of a Be/Si/Al mirror measured at an off-normal incidence angle of 2°.

reflectivity after a long-term storage. In the 17.1–40-nm wavelength range, this structure will be employed in the ARKA and KORTES solar research projects under preparation [19, 28].

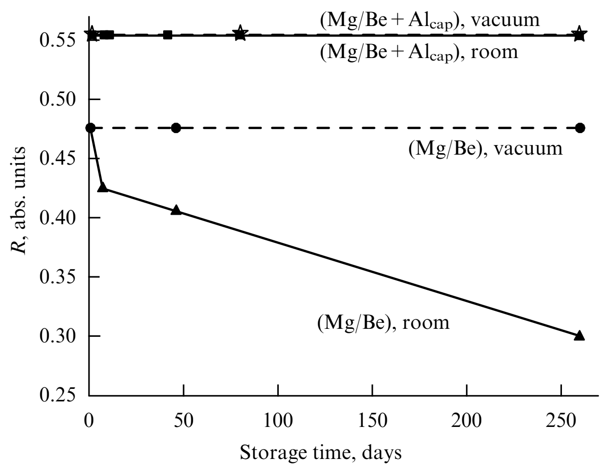

Figure 16. Comparison of the time dependences of the reflectivities of Mg/Be and Mg/Be + Al_{cap} MXMs stored under room conditions and in a forevacuum (at a pressure of 100 Pa).

As noted earlier, magnesium-based mirrors outperform aluminum-based ones from the standpoint of optical constants. However, magnesium-based mirrors are inherently unstable in X-ray optical characteristics, primarily due to the strong oxidation of magnesium. The VUV reflective characteristics of Be/Mg MXMs and their long-term stability were studied in Ref. [105]. Both simple two-component Mg/Be MXMs and structures with a thin protective aluminum capping film were studied. After synthesis, the mirrors were stored under different conditions: half of the samples were stored in room conditions and the other half in a forevacuum (residual atmosphere pressure: ~ 100 Pa). Figure 16 shows the dependences of the sample reflectivities at a wavelength of 30.4 nm on the observation time.

As is clear in Fig. 16, observed in the absence of a protective coating is a strong degradation of the reflectivity of Be/Mg MXMs. The reflectivity lowered from 49% to 30% in a period of nine months. Proceeding from the fact that the sample stored in a vacuum exhibited a high stability, it may be inferred that oxidation is the key factor responsible for reflectivity degradation.

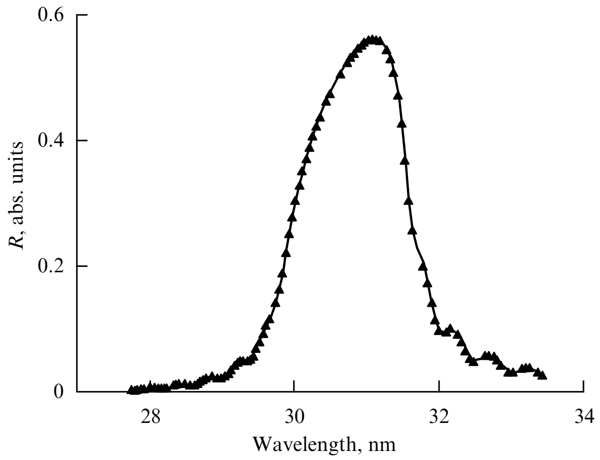

Figure 17. Spectral dependences of the reflectivity of $Mg/Be + Al_{cap}$ MXM samples stored in the atmosphere (symbols) and in a vacuum (solid curve).

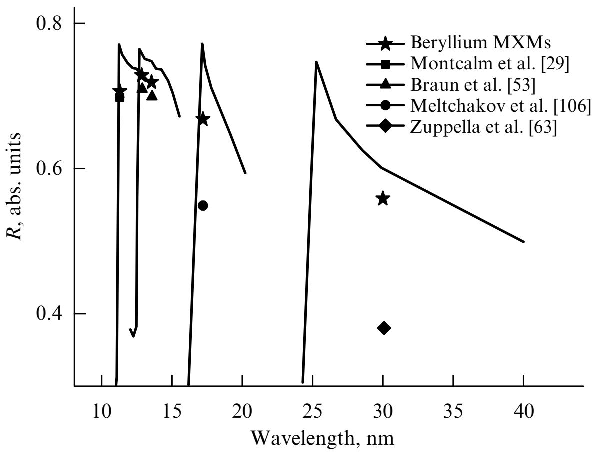

Figure 18. Record-breaking normal-incidence VUV mirror reflectivities. Asterisks stand for the data corresponding to beryllium-containing MXMs made at IPM RAS; other symbols denote data from Refs [29, 53, 63, 106]. Solid curves represent theoretical dependences.

Figure 17 shows the spectral dependences of the reflectivity of $Mg/Be + Al_{cap}$ MXM samples stored in the atmosphere (symbols) and in a vacuum (solid curve). The off-normal incidence angle was equal to 2°. The curves were recorded nine months after deposition. For a very good time stability, this structure possesses a record reflectivity $R = 56\,\%$ for a moderate transmission band $\Delta\lambda_{1/2} = 1.6$ nm ($\lambda/\Delta\lambda \approx 20$).

We characterize the contribution of beryllium-containing MXMs to modern multilayer X-ray optics of the VUV region. Figure 18 shows the record normal-incidence reflectivities of beryllium-based mirrors obtained at IPM RAS over the last four years (asterisks) and by other research groups earlier. As is evident from Fig. 18, all results in the 11–40-nm range surpassed the world level. In some spectral regions, the reflectivity was improved by nearly a factor of two.

6. Conclusions

The results of experimental investigations of beryllium-based MXMs for the 17.1–40-nm range testify to the efficiency of the idea to use Be as a scattering material proposed in Ref. [100]. Owing to their weak absorption, Be-based MXMs showed simultaneously record-breaking reflectivities and spectral selectivity, as well as the long-term stability of X-ray optical characteristics sufficient for practical applications. At wavelengths longer than the L absorption edge of Mg ($\lambda_L = 25.07$ nm), the reflectivities increased by nearly a factor of two in comparison with those for alternative MXM compositions. The mechanisms of the long-term stability of Be/Al mirrors and $Mg/Be + Al_{cap}$ mirrors with an aluminum protective layer are not quite clear. This is evidently related to the Al-on-Be boundary: in the case of Be/Mg samples with Al deposited on Mg, the barrier properties of Al vanish and the mirror degrades at almost the same rate as in the absence of a protective Al layer.

Beryllium turned out to be a useful material for lithography, both for a wavelength of 13.5 nm and for 11.3 nm. In this paper, we report for the first time about the achievement of a reflectivity $R = 71.2\,\%$ at the 11.3-nm wavelength using an $Mo/Be + Ru_{cap}$ MXM. The record-breaking reflectivity was achieved due to the protective capping Ru layer and the vacuum annealing of the structure. Among the unsolved problems is the relatively narrow transmission band of Mo/Be/Si MXMs at a wavelength of 13.5 nm and a relatively low (less than 70%) reflectivity of Ru/Be mirrors near the 11.3-nm wavelength. Preliminary results suggest that both of these problems may be solved by optimizing the Be-interlayer thickness and using B_4C interlayers at the second boundary in Mo/Si MXMs, as well as by introducing Mo interlayers in Ru/Be.

Due to its low SXR absorption, low density and low atomic number, beryllium provides a high optical contrast with practically all materials. Therefore, Be is highly promising for this wavelength range. In subsequent investigations, a study will be made of Cr/Be, Ni/Be, and W/Be MXMs for the wavelength range of 0.01–4 nm. The first experimental data outlined in Ref. [107] suggest that research in this direction is promising.

In conclusion, we note that all resultant record data emphasize the modern trend in multilayer X-ray optics development: the use of barrier layers inside an MXM and protective capping layers. The time of simple two-layer systems has already passed. And so the revision of previously obtained results with MXMs that have become 'classical' is a topical task, which may result in a significant improvement in their X-ray optical characteristics.

Acknowledgements
This work was performed with the use of equipment from the Physics and Technology of Micro- and Nanostructures Shared Equipment Centre of IPM RAS in the framework of the State Assignment for IPM RAS (project no. 0035-2014-0204) with support from the Russian Foundation for Basic Research (grant nos 19-07-00173, 19-02-00081, 18-02-173, 18-02-00588, 17-52-150006, 18-42-520007, 18-32-00671, and 18-32-00173).

References

1. Schuster M, Gobel H *J. Phys. D* **28** A270 (1995)
2. Underwood J H, Barbee T W (Jr.) *Nature* **294** 429 (1981)
3. Störmer M et al. *J. Synchrotron Rad.* **25** 116 (2018)
4. Störmer M et al. *Rev. Sci. Instrum.* **87** 051804 (2016)
5. Bilderback D H et al. *J. Synchrotron Rad.* **7** 53 (2000)
6. Takacs P Z *Synchrotron Radiat. News* **2** 24 (1989)
7. Chkhalo N I et al. *Nucl. Instrum. Meth. Phys. Res. A* **359** 121 (1995)
8. Zhang L et al. *J. Phys. Conf. Ser.* **425** 052029 (2013)

9. Windt D L, Bellotti J A *Appl. Opt.* **48** 4932 (2009)
10. Jonnard P et al. *Proc. SPIE* **7360** 73600O (2009)
11. Windt D L et al. *Proc. SPIE* **5168** 1 (2004)
12. Li H et al. *Proc. SPIE* **7995** 79951E (2010)
13. Bogachev S A et al. *Appl. Opt.* **55** 2126 (2016)
14. Wu W-J et al. *Chinese Phys. Lett.* **28** 086801 (2011)
15. Beigman I L, Pirozhkov A S, Ragozin E N *JETP Lett.* **74** 149 (2001); *Pis'ma Zh. Eksp. Teor. Fiz.* **74** 167 (2001)
16. Kuhlmann T et al. *Proc. SPIE* **4782** 196 (2002)
17. Vishnyakov E A et al. *Quantum Electron.* **42** 143 (2012); *Kvantovaya Elektron.* **42** 143 (2012)
18. Okajima T et al. *Appl. Opt.* **41** 5417 (2002)
19. Shestov S V et al. *Proc. SPIE* **9144** 91443G (2014)
20. Yamashita K et al. *Appl. Opt.* **37** 8067 (1998)
21. Hecquet C et al. *Appl. Phys. A* **95** 401 (2009)
22. Barysheva M M et al. *Quantum Electron.* **49** 380 (2019); *Kvantovaya Elektron.* **49** 380 (2019)
23. Wonisch A et al. *Appl. Opt.* **45** 4147 (2006)
24. Pirozhkov A S, Ragozin E N *Phys. Usp.* **58** 1095 (2015); *Usp. Fiz. Nauk* **185** 1203 (2015)
25. Garakhin S A et al. *Quantum Electron.* **47** 378 (2017); *Kvantovaya Elektron.* **47** 378 (2017)
26. Kortright J B, Underwood J H *Nucl. Instrum. Meth. Phys. Res. A* **291** 272 (1990)
27. Andreev S S et al. *Nucl. Instrum. Meth. Phys. Res. A* **543** 340 (2005)
28. Kuzin S V et al. *Izv. Ross. Akad. Nauk, Ser. Fiz.* **75** 91 (2011)
29. Montcalm C et al. *Proc. SPIE* **3331** 42 (1998)
30. Sae-Lao B, Montcalm C *Opt. Lett.* **26** 468 (2001)
31. Tsarfati T et al. *Thin Solid Films* **518** 1365 (2009)
32. Andreev S S et al. *Nucl. Instrum. Meth. Phys. Res. A* **603** 80 (2009)
33. Platonov Y et al. *Proc. SPIE* **8076** 80760N (2011)
34. Panessa-Warren B J, in *X-Ray Microscopy. Proc. of the Intern. Symp., Gottingen, Fed. Rep. of Germany, September 14–16, 1983* (Eds G Schmahl, D Rudolph) (Berlin: Springer-Verlag, 1984) p. 268; Translated into Russian: *Rentgenovskaya Optika i Mikroskopiya* (Moscow: Mir, 1987) p. 359
35. Kirz J, Jacobsen C, Howells M *Q. Rev. Biophys.* **28** 33 (1995)
36. Barysheva M M et al. *Phys. Usp.* **55** 681 (2012); *Usp. Fiz. Nauk* **182** 727 (2012)
37. Vinogradov A V et al. *Pis'ma Zh. Tekh. Fiz.* **13** 129 (1987)
38. Renner O et al. *Rev. Sci. Instrum.* **63** 1478 (1992)
39. Takahashi J et al. *Rev. Sci. Instrum.* **60** 2024 (1989)
40. Skulina K M et al. *Appl. Opt.* **34** 3727 (1995)
41. Mirkarimi P B et al. *Appl. Opt.* **39** 1617 (2000)
42. Singh M, Braat J J M *Appl. Opt.* **39** 2189 (2000)
43. Bajt S *J. Vac. Sci. Technol. A* **18** 557 (2000)
44. Soufli R et al. *Proc. SPIE* **3767** 251 (1999)
45. Akhsakhalyan A D et al. *Poverkhnost* (1) 5 (2017)
46. Salashchenko N N, Chkhalo N I *Herald Russ. Acad. Sci.* **78** 279 (2008); *Vestn. Ross. Akad. Nauk* **78** 450 (2008)
47. Churilov S S et al. *Phys. Scr.* **80** 045303 (2009)
48. Wagner C, Harned N *Nature Photon.* **4** 24 (2010)
49. Otsuka T et al. *Appl. Phys. Lett.* **97** 231503 (2010)
50. Tsarfati T et al. *Altern. Lithogr. Technol.* **7271** 72713V (2009)
51. Chkhalo N I et al. *Appl. Phys. Lett.* **102** 011602 (2013)
52. Chkhalo N I, Salashchenko N N *AIP Adv.* **3** 082130 (2013)
53. Braun S et al. *Jpn. J. Appl. Phys.* **41** 4074 (2002)
54. Bajt et al. S *Opt. Eng.* **41** 1797 (2002)
55. Nyabero S L et al. *J. Appl. Phys.* **112** 054317 (2012)
56. Yamamoto M et al. *J. Jpn. Soc. Precis. Eng.* **52** 1843 (1986)
57. Corso A J et al. *Opt. Express* **19** 13963 (2011)
58. Nii H et al. *J. Synchrotron Rad.* **5** 702 (1998)
59. Hu M-H et al. *Opt. Express* **18** 20019 (2010)
60. Zuev S Yu et al. *Bull. Russ. Acad. Sci. Phys.* **74** 50 (2010); *Izv. Ross. Akad. Nauk. Ser. Fiz.* **74** 58 (2010)
61. Polkovnikov V N et al. *Tech. Phys. Lett.* **45** 85 (2019); *Pis'ma Zh. Tekh. Fiz.* **45** (2) 26 (2019)
62. Fernández-Perea M et al. *Opt. Express* **20** 24018 (2012)
63. Zuppella P et al. *Proc. SPIE* **8076** 807608 (2011)
64. Aquila A et al. *Opt. Express* **17** 22102 (2009)
65. Galtayries A et al. *Surf. Interface Anal.* **42** 653 (2010)
66. Henke B L, Gullikson E M, Davis J C *At. Data Nucl. Data Tables* **54** 181 (1993)
67. Bibishkin M S et al. *Nucl. Instrum. Meth. Phys. Res. A* **543** 333 (2005)
68. Andreev S S et al. *J. Synchrotron Rad.* **10** 358 (2003)
69. Chkhalo N I, Salashchenko N N, Zorina M V *Rev. Sci. Instrum.* **86** 016102 (2015)
70. Barysheva M M et al. *Izv. Ross. Akad. Nauk. Ser. Fiz.* **75** 71 (2011)
71. Asadchikov V E et al. *Prib. Tekh. Eksp.* (3) 99 (2005)
72. Svechnikov M et al. *J. Appl. Cryst.* **50** 1428 (2017)
73. Volkov Yu O et al. *Crystallogr. Rep.* **58** 160 (2013); *Kristallografiya* **58** 146 (2013)
74. Lee P *Appl. Opt.* **22** 1241 (1983)
75. Vinogradov A V, Kozhevnikov I V *Tr. Fiz. Inst. Akad. Nauk SSSR* **196** 62 (1989)
76. Névot L, Croce P *Rev. Phys. Appl.* **15** 761 (1980)
77. Stearns D G *J. Appl. Phys.* **65** 491 (1989)
78. Kozhevnikov I V *Nucl. Instrum. Meth. Phys. Res. A* **498** 482 (2003)
79. Holý V, Baumbach T *Phys. Rev. B* **49** 10668 (1994)
80. Andreev S et al. *Open Phys.* **1** 191 (2003)
81. Bibishkin M S et al. *Proc. SPIE* **5401** 8 (2004)
82. Garakhin S A et al. *Quantum Electron.* **47** 385 (2017); *Kvantovaya Elektron.* **47** 385 (2017)
83. Schäfers F et al. *J. Synchrotron Rad.* **23** 67 (2016)
84. Sokolov A et al. *Rev. Sci. Instrum.* **87** 052005 (2016)
85. Langford R M, Petford-Long A K *J. Vac. Sci. Technol. A* **19** 2186 (2001)
86. Chkhalo N I et al., in *Nanofizika i Nanoelektronika. Trudy XXII Mezhdunarodnogo Simpoziuma, 12–15 Marta 2018 g., Nizhny Novgorod* (Nanophysics and Nanoelectronics. Proc. of the XXII Intern. Symp., March 12–15, 2018, Nizhny Novgorod) (Nizhny Novgorod: Izd. Nizhegorodskogo Gos. Univ. im. N.I. Lobachevskogo, 2018) p. 494; http://nanosymp.ru/UserFiles/Symp/2018_v1.pdf
87. Svechnikov M V et al. *Opt. Express* **26** 33718 (2018)
88. Drozdov M N et al. *Pis'ma Zh. Tekh. Fiz* **38** (24) 75 (2012)
89. Ber B et al. *Thin Solid Films* **540** 96 (2013)
90. Tolstoguzov A B *J. Anal. Chem.* **65** 1370 (2010)
91. Drozdov M N et al. *Thin Solid Films* **577** 11 (2015)
92. Drozdov M N et al. *Thin Solid Films* **661** 65 (2018)
93. Nechay A N et al. *AIP Adv.* **8** 075202 (2018)
94. Drozdov M N et al. *Poverkhnost* (5) 50 (2010)
95. Stamm U et al. *Proc. SPIE* **5037** 119 (2003)
96. Rakowski R et al. *Appl. Phys. B* **101** 773 (2010)
97. Banine V Y et al. *J. Phys. D* **44** 253001 (2011)
98. Pirati A et al. *Proc. SPIE* **10143** 101430G (2017)
99. Yakshin A E et al. *Proc. SPIE* **6517** 65170I (2007)
100. Chkhalo N I et al. *Thin Solid Films* **631** 106 (2017)
101. Chkhalo N I et al., in *Physics of X-Ray and Neutron Multilayer Structures Workshop, Univ. Twente, The Netherlands, 2016*; https://www.utwente.nl/mesaplus/xuv/workshops/archive/pxrnm-workshop-2016/program/chkhalo-structural-and-reflective-characteristics-of-mo-be-multilayer-with-barrier-layers.pdf
102. Chkhalo N I et al. *Opt. Lett.* **42** 5070 (2017)
103. Zuev S Yu et al. *Poverkhnost* (3) 5 (2019)
104. Chkhalo N I et al. *J. Nanosci. Nanotechnol.* **19** 546 (2019)
105. Polkovnikov V N et al. *Opt. Lett.* **44** 263 (2019)
106. Meltchakov E et al. *Proc. SPIE* **8168** 816819 (2011)
107. Akhsakhalyan A A et al. *Poverkhnost* (1) 14 (2019)